Applied Surface Science 491 (2019) 792–798

Contents lists available at ScienceDirect

Applied Surface Science

journal homepage: www.elsevier.com/locate/apsusc

Full length article

Elucidating the role of extended surface defects at Fe surfaces on CO adsorption and dissociation

Aurab Chakrabarty[a], El Tayeb Bentria[b], Salawu Akande Omotayo[c], Othmane Bouhali[c], Normand Mousseau[d], Charlotte S. Becquart[e], Fedwa El Mellouhi[b,*]

[a] Department of Physics, Nims University Rajasthan, Jaipur, India
[b] Qatar Energy and Environment Research Institute, Hamad Bin Khalifa University, Po Box 34110, Doha, Qatar
[c] Science Program, Texas A&M University at Qatar, Doha, Qatar
[d] Département de physique, Université de Montréal, Montréal, Canada
[e] UMET, UMR 8207, ENSCL, Université Lille 1, Lille, France

ARTICLE INFO

Keywords:
Iron surface
CO adsorption
CO dissociation
Metal dusting corrosion
Surface vacancy clusters
Grain boundary
Reactive force field

ABSTRACT

The adsorption and dissociation of hydrocarbons on metallic surfaces during catalytic reactions in a steam reforming furnace often lead to the carburization of the catalysts and metallic surfaces involved. This process is greatly accelerated by the presence of intrinsic defects like vacancies and grain boundaries and is succeeded by surface to subsurface diffusion of C. We employ both density functional theory and reactive force field molecular dynamics simulations to investigate the effect of surface defects on CO dissociation rate directly related to metal dusting corrosion. We demonstrate that stable surface vacancy clusters with large binding energies accelerate the adsorption of CO molecules by decreasing the corresponding dissociation energies. In addition, we demonstrate that the appearance of multiple GBs at the surface leads to an enhancement of the CO dissociation rate. Furthermore, we demonstrate that the increase in surface roughness by emerging GBs leads to an increase in CO dissociation rate.

1. Introduction

Carburization is considered as the initiating process for dusting corrosion, a phenomenon that causes major problems in the internal part of hydrocarbon transport pipelines, for example. A detailed and complete understanding of the carburization process is much sought-after owing to its economic implications. There are several studies [1] that examine the factors that would affect the carburization mechanism under realistic conditions such as the structural composition of the alloys (consisting of Fe, C, Mn, Cr and Ni) and the presence of unwanted impurities such as H, N, S and O. The reaction of CO with the Fe surface is one of the most basic carburization reactions [2,3] studied by several first-principles methods. Previous studies confirm that the presence of H adatoms on the Fe surfaces accelerates the dissociation of CO [4], while the presence of O and H_2O reduces the reaction yield [5]. However, in a realistic scenario, one must also consider inherent defects that are abundant on and beneath the surface, and that can affect the (i) adsorption (ii) dissociation of the hydrocarbons, and (iii) diffusion of carbon into the subsurface. In a previous work [6], we showed that vacancy defects are easily formed on the Fe surface and readily accelerate all the three sub-processes of carburization mentioned above. Specifically, the presence of a single vacancy defect at the surface causes the adsorption of CO to become energetically favorable by 20–50 meV, while the dissociation barrier is reduced by 200–360 meV [6]. We have also investigated by means of Density functional theory (DFT) and with ReaxFF the effect of emerging Σ3 and Σ5 grain boundaries and their grooves on CO dissociation rate. We showed that the groove area generated by these grain boundaries (GB) on surface enhance the CO dissociation rate, depending on the type of surface cleaved [7].

Vacancy defects are known for self-segregation leading to the creation of voids that act as trap centres for alloying atoms and pinning centres for larger defects such as dislocations thus affecting the overall structural properties [8,9]. Positron annihilation spectroscopy experiments reveal that several single Fe vacancies on the surface can be mobile at room temperature and migrate through the crystal to form a vacancy cluster or supervacancy [10]. This migration is driven by the lower defect formation energy at the edge of a void with respect to bulk [9,11]. This also explains the low vacancy formation energy on a Fe (110) surface [6]. Besides voids, certain grain boundaries (GB)

* Corresponding author.
E-mail address: felmellouhi@hbku.edu.qa (F. El Mellouhi).

https://doi.org/10.1016/j.apsusc.2019.05.278
Received 9 December 2018; Received in revised form 22 May 2019; Accepted 23 May 2019
Available online 25 May 2019
0169-4332/

emerging toward the surface [12,13] can also act as a trap centre for adsorbate molecules. In addition, voids might result from the intersection of these GBs consequently leading to pit initiation [14]. Recently, Lu et al. [15] showed that grain boundaries are major drivers of carbon diffusion in bulk iron [15]. Therefore, a surface-emerging GB is expected to accelerate dissociation of CO molecules and sometimes the surface-to-subsurface diffusion of C by acting as a channel [7].

In this work, we study large defects that alter the topology of the iron surface at the nanoscale and elucidate their effects on the adsorption and dissociation of CO. In addition to DFT, we use the ReaxFF empirical potential [16]. This approach enables us to scale up the DFT model in order to work with a large atomistic model that can accommodate extended surface defects and alleviate the constrains emerging from image interaction due to periodic boundary conditions. We first validate the reliability of the ReaxFF potential by comparing its prediction to that of DFT for surface and defect formation energies as well as adsorption and dissociation energies of CO molecules. Next, we model two extended surface defects: i) partially peeled surface resulting in vacancy clusters where up to 9 atoms are removed from the surface to form small voids; ii) a collection of grain boundaries emerging at the surface and constructed from a cleaved polycrystalline system. The two extended surface defects on the iron surface explored here can be considered as a sample of intrinsic nanoscale defects that may exist on the surface leading to dusting pit initiation.

2. Computational methods

Density functional theory (DFT) [17] calculations were performed using the Vienna *Ab-initio* Simulation Package (VASP) [18] with cutoff energy of 520 eV and using the projector-augmented wave (PAW) pseudopotential [19] together with PBE exchange-correlation functional [20]. Surface slab supercells with a sufficiently large surface area were chosen in order to prevent periodic image-interaction of adsorbates. For the (110) slab, a 7 layer-thick 4×4 multiple of the surface periodic unit cells was chosen with a surface area of 96 $Å^2$ and a vacuum of 20 Å along the *z*-direction. Full relaxation of the slab containing a total of 112 atoms was undertaken by allowing the iron atoms within the top 4 layers to relax while the remaining layers were kept fixed during energy minimization. A k-point mesh was automatically generated using Monkhorst-Pack grid of $7 \times 7 \times 1$ mesh. Ionic relaxation steps were performed using convergence criteria of 10^{-4} eV/atom and 10^{-3} eV for forces and total energy respectively. The Nudged elastic band (CI-NEB) method [23] was used to obtain the dissociation and diffusion pathways using between 7 and 11 images, with a convergence force tolerance of 0.001 eV/Å and a coarser k-point mesh of $5 \times 5 \times 1$.

For non-dynamical calculation of CO dissociation on the (110) surface, simulation setups similar to the DFT condition have been selected. The Halgren-Lipscomb method is used to generate the initial CI-NEB path as implemented in QuantumWise [24], then climbing-image nudged elastic band (CI-NEB) method was used to optimize the minimum energy paths (MEP).

Molecular dynamics simulations (MD) were performed with the LAMMPS package using the interatomic bond-order reactive force field (ReaxFF) [16]. The equations of motion were integrated using the velocity-Verlet algorithm in the canonical ensemble (NVT). Periodic boundary conditions (PBC) were applied along the three Cartesian coordinates, a vacuum of 16 Å along the *z*-direction was used to simulate a well isolated slab, and allow the insertion of molecules. A 10×5 multiple of the surface periodic unit cells was chosen resulting in a surface area of 465 $Å^2$, with 8 layer-thick. For the multiple-grain boundary systems, we used a simulation box of 1519 $Å^2$ surface area, resulting in a system of 2200 atoms on average, with 30 Å of vacuum slab. The VNL-ATK code by Quantumwise [21] was used to generate multi-grain systems by means of Polycrystalline Voronoi builder [22], while respecting the continuity of boundary condition in the three directions. Since we are dealing with a system with vacuum, we created a wall perpendicular to the *z*-direction to keep the interaction within one of the surfaces only. The "deposit" command was used to insert molecule into the vacuum region to probe the catalytic dissociation of CO every 2500 steps while avoiding the formation of complex hydrocarbons in the vacuum region. A time step of 0.2 fs was selected based on our validated earlier simulation setup [7]. Simulations were run for up to 300 ps; during the equilibration stage and after structural optimization, temperature was raised gradually by 0.01 K per MD step. The dissociation rate was calculated using a simple script that reads MD dumping files at the required time step and calculates the distance between C and O atoms [7].

3. Results

3.1. Iron surface relaxation

Before exploring the adsorption and dissociation on these surfaces, it was essential to validate the basic characteristics of these surfaces by accurately reproducing them using the ReaxFF potential. For this, we calculated the surface energy and the reconstruction parameter δz_n for the top layers of the surfaces relevant to this work: surfaces parallel to the (110), (111) and (210) planes. This parameter is defined as the percentage change in the n^{th} layer-separation with respect to that for bulk Fe. The reconstruction parameter indicates the convergence of the relaxation after the surface cleavage and confirms that the thickness of the supercell used in these calculations is sufficient. This parameter was calculated using both DFT and ReaxFF as shown in Table 1 where we compare our calculated values with available data from the literature. As can be seen in Table 1, all three surfaces have similar surface energies and are converged within the 5th layer with the change in the interlayer spacing $\delta z_5 < < 1\%$. The ReaxFF potential is thus able to well reproduce the surface property in agreement with DFT. Even though we observe that the layers closer to surface are more relaxed, while the deeper layers are comparatively rigid, the surface energies obtained by ReaxFF remain in very good agreement with the DFT calculated ones.

Table 1
Surface energies E_{surf} and reconstruction parameter of the nth layers δz_n for Fe cleaved along (110), (111), and the (210) surfaces calculated with DFT and ReaxFF.

Surface		E_{surf} (J/m^2)	δz_1	δz_2	δz_3	δz_4	δz_5
(110)	DFT	2.44[a], 2.37[b]	+0.04[a], 0.10[b]	+0.11[a], +0.30[b]	−0.22[a],-0.01[b]	−0.08	+0.03
	ReaxFF	2.18	−0.65	+0.35	−0.16	−0.10	+0.01
(111)	DFT	2.80[a], 2.58[b]	−12.65[a],-17.7[b]	−9.75[a], 8.40[b]	−2.91[a], +11.0[b]	−5.85[a],-1.01[b]	−0.63[a],-0.50[b]
	ReaxFF	2.74	−21.65	−12.02	+2.12	−0.23	−0.09
(210)	DFT	2.57[a], 2.60[b]	−19.11[a], 23.0[b]	−5.50[a], 5.60[b]	+15.31[a], +15.30[b]	−6.04[a],-8.20[b]	+0.26[a],-2.40[b]
	ReaxFF	2.49	−21.98	−9.36	+6.65	−1.65	−0.12

[a] This work.
[b] Data taken form reference [25].

3.2. Energetics of surface vacancy clusters

Individual single vacancies in bulk Fe and Ni are known to migrate to form a large void or supervacancy [9], and similar behaviour is expected from surface vacancies that tend to coalesce and segregate to form vacancy clusters on the surface.

The formation energy of n vacancies was calculated using:

$$E_v^f = E_f - \left[\frac{N_0 - n}{N_0}\right]E_i$$

where N_0 is the initial total number of atoms in the cell, E_i is the initial energy, n is the number of Fe atoms removed and E_f represents the final energy. The reference for the self-energy term of the vacancy formation energy is usually the energy of a single atom in bulk. Due to bonding, this represents an energy different from that of a single atom in vacuum. However, in this particular case, we are estimating the vacancy formation energy of a surface atom, which is intuitively lower than that in bulk. Therefore, for a fair comparison, one must subtract the energy of a surface atom. Since our goal is to compare surface vacancies, a relative value of formation energy will suffice.

The (110) surface is the most densely packed and has been dubbed the 'most reactive' surface for bcc structure [6]. It is therefore primarily considered in this work. Note that the single vacancy formation energy on the (110) surface is 0.9 eV which is much smaller than for the bulk, *i.e.* ~2 eV [26–28]. This being said, various topologies of surface vacancies might exist. We explored the topology of vacancy clusters on the (110) surface using the ReaxFF by increasing the number of vacancies to create clusters containing between one to nine vacancies. Due to a large Fe—Fe interlayer separation of 2.02 Å compared to the in-plane distance of 1.4 Å, a peeled vacancy cluster (with only surface atom removed) has a much smaller formation energy than a cluster consisting of vacancies removed from the first and second layers. For example, the formation energy of a 5-vacancy cluster as a 'peeled layer' on surface is 2.7 eV, when the 5 nearest neighbour atoms on the (110) surface layer are removed. On the other hand, the energy cost for an indent-shaped defect, *i.e.* 4 surface atoms and one subsurface atom directly beneath them are removed, is 11.5 eV. Small indent-shaped clusters have a negative segregation energy, which implies that these vacancy clusters are less favorable than individual vacancy defects with the same number of atoms removed. It might appear intuitive that the roughness of the surface would enhance the CO dissociation rate by exposing greater surface area. Nevertheless, entropic effects induce an extensive purging of surface extended defects and roughness, suggesting that only the nano-scale defects that are associated with a relatively low formation energy persist. Because of this instability, we did not pursue our investigation of indent-shaped surface vacancy clusters.

We have observed that the formation energy of a peeled vacancy cluster is always lower than that of multiple non-interacting single defects. The formation energy difference between these configurations represents the energy gain associated with surface vacancy segregation. Fig. 1 compares the formation energy of segregated vacancies on a (110) surface for DFT and ReaxFF. ReaxFF results are in quantitative agreement with the DFT, enabling us to scale up the calculation to larger systems containing up to 9 aggregated and non-aggregated vacancies. Both approaches indicate that vacancies prefer to cluster on the surface, as the formation energy of a cluster containing n vacancies is lower than n times the formation of the isolated vacancy. The difference in these two formation energies represents the energy gain associated with aggregation that reaches up to 5 eV in the case of 9 vacancy clusters calculated with ReaxFF.

3.3. CO adsorption and dissociation pathways near surface vacancy clusters

The molecular adsorption of CO on the surface is the first step in carburization leading to the initiation of dusting corrosion of a metal.

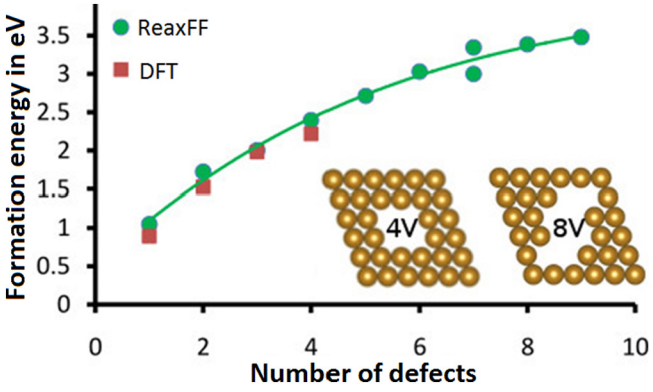

Fig. 1. Calculated formation energy (in eV) of segregated vacancies using ReaxFF (green circles) and DFT (red squares) as function of the number of vacancies. This plot shows the energetics of the most stable arrangement of extended vacancy defects as a function of the number of vacancies. Only the formation energy of the most stable extended defect arrangement is shown, except for the case of 7 vacancies where two arrangements of the vacancies seem to be very close in energy. The atomistic models at the bottom of the figure show two representative stable vacancy arrangements for 4 and 8 vacancies respectively. Fe is yellow, blank represents the vacancies. (For interpretation of the references to color in this figure legend, the reader is referred to the web version of this article.)

Adsorption energies of CO on different sites close to single and cluster vacancies compared to a clean surface are given in Table S1. For each system, the energies are given relative to the minimum adsorption energy configuration, which is set as reference. Based on the DFT calculations, the preferred adsorption site on a clean surface is the on-top (OT) site followed by an adsorption site at the threefold (TF) which is only 20 meV higher. The hollow site (H) follows with 30 meV higher energy than minimum energy adsorption site while the bridge stands 170 meV higher in energy. The adsorption in the presence of vacancies is much more selective, strongly favouring the TF site compared to the other OT and B sites lying hundreds of meV higher in energy. The hollow site sitting on top of four iron atoms cannot be defined in the vicinity of the vacancy because of the missing atoms. The migration path of the CO molecule from a TF site far from a single vacancy defect to the lowest energy site next to the vacancy (TF ➔ TF) is shown in the ESI (Fig. S1). A migration barrier of 0.2 eV leads to trapping of the CO molecule at a TF site in the vicinity of the vacancy which is 0.6 eV more stable. This trapping near the vacancy is a consequence of a stronger C—Fe bond formation.

Interestingly, one notices that the energy difference between the TF minimum energy configuration and the OT and B sites increases as the vacancy void grows suggesting a strong trapping at the TF site near the vacancy clusters. Contrary to the Fe-C-O bond angle of 90° the adsorbed CO molecule makes on the clean surface [6], a steep Fe-C-O bond angle of 34° manifests when a CO molecule is adsorbed next to a single vacancy. This is also observed for the 4-vacancy cluster with a slightly steeper 39° angle. This is apparent from Fig. 2 where a cross-section of the electronic localization functions (ELF) is shown. The features of Fe-C-O bond angle, bond formation and electronic exchange of CO adsorbed on a clean Fe surface and at the edge of a vacancy cluster respectively confirm the strong covalent character of the bonds. The vacancy trapping effect is mediated by the rearrangement of iron around the vacancy cluster enabling a more efficient electronic transfer from the surface toward the highly electronegative O atom [6].

Overall, the ReaxFF potential is in qualitative agreement with DFT by identifying TF as the lowest adsorption site near the vacancy clusters. It is worth mentioning that the ReaxFF empirical potential calculations predict angles of 36° and 47° for single and 4-vacancy clusters, respectively, in a very reasonable agreement with DFT. A small discrepancy is however identified for the clean surface where it identifies

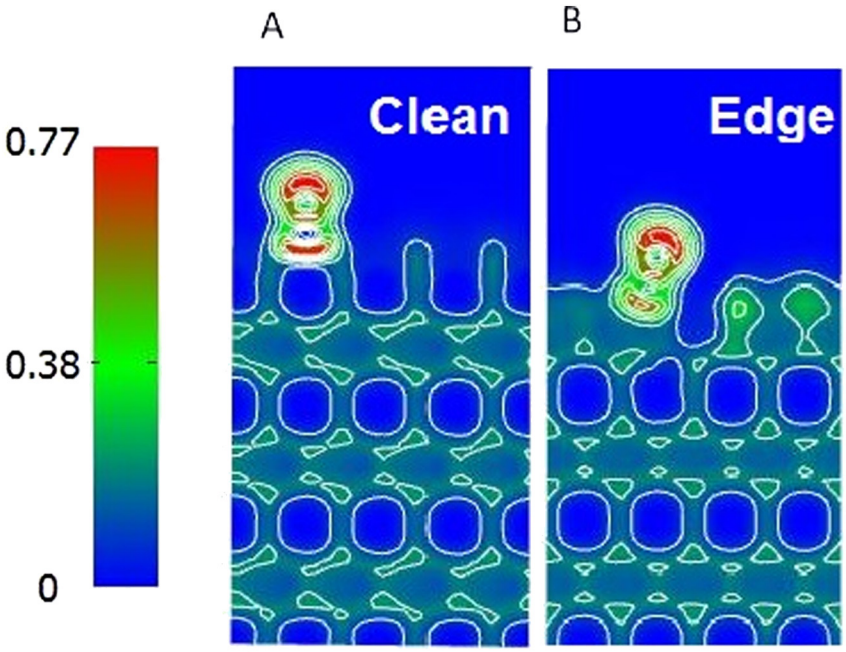

Fig. 2. Cross section of the electronic localization function (ELF) showing a CO molecule adsorbed on (A) a clean surface and on (B) the edge of a 4-vacancy cluster edge.

the TF as the lowest instead of the OT found in the DFT calculations. The ReaxFF OT site shows the largest deviation from the DFT results, suggesting that the potential manifests some discrepancies at this particular adsorption site.

The CI-NEB dissociation pathway shown in Fig. 3-A is for a large supercell with a single CO molecule on 4 × 4 iron (110) slab, which was chosen here to minimize the finite size-effects [6]. We showed in an earlier work that the dissociation barrier is reduced in the presence of a single vacancy because of the strong vacancy-carbon attraction. However, we have also shown that the high electron-affinity of the O atom slightly increases the dissociation barrier in the vicinity of an electron-deficit void [6]. The calculated dissociation barriers on the clean surface are 0.77 eV for ReaxFF and 0.78 eV with DFT, showing a remarkably good agreement between the two methods.

Regarding the CO dissociation at the edge of the vacancy, the DFT pathways is characterized first by a barrier for the migration from the most stable site quasi-threefold to the neighbouring on-top local minimum which is 0.25 eV higher, followed by an additional barrier of dissociation of 0.38 eV leading to surface to subsurface diffusion. The overall barrier with DFT (migration + dissociation) is 0.63 eV. However, with Reaxff, the on-top configuration is 1.54 eV higher than the minimum making it hardly accessible compared to the 0.25 eV energy difference with DFT. The threefold site-adsorbed configuration next to the vacancy (edge of the vacancy) is the minimum energy adsorption configuration for both the single and the cluster vacancy: see Table S1 in the Supplementary Information. Therefore, the CO molecule can dissociate in a way almost identical to the process happening in the vicinity of a single vacancy. The CI-NEB pathway using ReaxFF does not

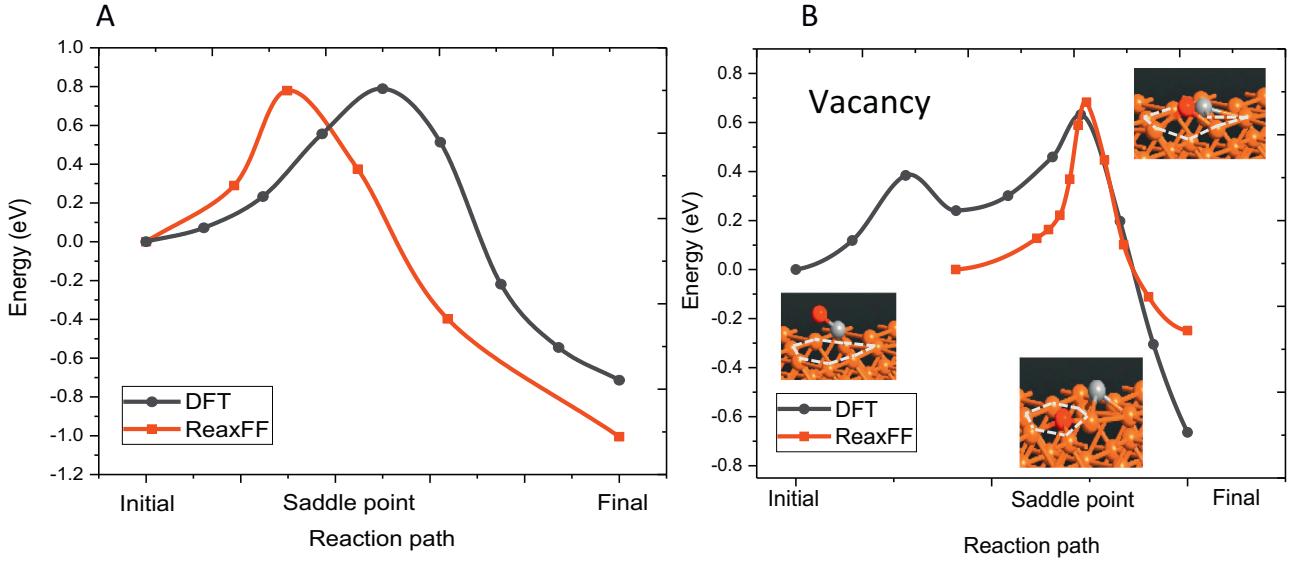

Fig. 3. The CO dissociation pathways on a Fe(110) surface calculated with DFT and ReaxFF for (A) a clean surface and (B) a surface with a single vacancy (white dash lines). The atomistic models show the initial and final states where Fe is brown, carbon is grey and oxygen is red. (For interpretation of the references to color in this figure legend, the reader is referred to the web version of this article.)

require the same migration as DFT and the molecule adsorbed on the quasi-threefold site minimum dissociates with a barrier of 0.68 eV as presented in Fig. 3-B. It is also worth mentioning that ReaxFF could not capture the relaxation of the carbon atom after dissociation by moving from the surface to the vacancy subsurface and stays at the top, which is reflected on the final energy on Fig. 3-B. This artefact has been reported in our earlier work [7] and is believed not to affect the dynamics when running short simulations.

Moreover, we conducted CI-NEB calculation of CO dissociation on a step-edge using ReaxFF and obtained a barrier as low as 0.62 eV, from the adsorption of CO on the nearest TF position to the step-edge, to the fully dissociated oxygen atom at the step-edge (see Fig. S2 in the ESI).

3.4. Effect of surface roughness on CO dissociation rate

We have shown that the ReaxFF potential is capable of reproducing the results obtained with DFT and captures the essential trends during finite temperature dynamics. Hence, we were able to scale-up the simulation from atomic to nano-scale. This allowed us to explore complex systems that include a combination of different types of surface defects on polycrystalline iron structures such as atomically large voids, step edges as well as emerging GBs. These systems, counting between 700 and > 2200, are too expensive computationally for DFT, thus the next section is restricted to molecular dynamic simulation using the previously tested ReaxFF potential. The finite temperature MD evolution of the Fe-CO system under diverse conditions enables us to capture at the same time the i) CO dissociation, ii) diffusion of carbon and oxygen atoms to the subsurface and iii) the formation of carbides. In order to get insight to the dusting corrosion rate, our main focus will be to quantify the CO dissociation rate, a fundamental property that describes the reactivity of the surface that is closely related to the corrosion rate [23]. The dissociation rate in this work was calculated with respect to bond-breaking with the assumption that a C—O distance larger than 1.6 Å records a dissociation event of the CO molecule [23] .

The CO dissociation pathway presented in Fig. 4 at 500 K shows that the surface vacancy clusters contribute to the enhancement of the CO dissociation rates and thus metal dusting. The surface reconstruction of iron atoms affects the CO dissociation rate as evidenced from the difference in CO dissociation rate between two systems with the same density of vacancies, but with different surface reconstructions (see Fig. 4-C). The CO dissociation for the 9-vacancy cluster is up to 35% higher than that on the clean surface after 300 ps simulation time (Fig. 4-C).

Fig. S3 in the ESI, shows top view MD snapshots of a vacancy cluster defect on a (110) surface. The CO dissociation in and around the vacancy and the C atom displacement into the subsurface due to iron atoms restructuring are clearly visible. The temperature effect on the dissociation in a defective system is not surprisingly different from that of a clean system and follows the Arrhenius rule.

Next, we examine grain boundary (GB) edges and grooves that also provide various reduced-energy CO adsorption sites [7]. Multi-GBs surface represent a cleave exposing the polycrystalline nature of the metal. It can be considered an example of extreme roughness of a surface. Fig. 5 shows the (110) clean surface together with a cleaved polycrystalline iron system composed of (2, 4 and 6 grains) emerging at the surface. The structures were generated using the Polycrystalline Voronoi builder available in VNL package [30]. This method is based on random closed packing of spheres. Geometrical and topological properties obtained with it were shown to compare well with properties of real polycrystalline materials [22].

In order to examine the effect of temperature and surface roughness, we conducted MD simulations at ambient (300*K*) and high temperature (800 K), for both the multi-GB models and free (110) surfaces. In our earlier work [7], we had found that 800 K represents the temperature that leads to the highest CO dissociation rate (which corresponds experimentally to the high metal dusting corrosion rate) [7]. Fig. 6 shows the CO dissociation rate as a function of time at these conditions for both simulated temperatures. The behaviour of the CO dissociation rate for the clean and rough surfaces is similar: i) the dissociation rate increases rapidly with the insertion of molecules, ii) after full insertion, the dissociation rate slows down before saturating.

Turning to the effect of surface roughness, differences can be observed on the 300 K CO dissociation rate plots (Fig. 6a). The probability for CO molecules to adsorb followed by their dissociation increases progressively with increasing the density of available adsorption sites in the vicinity of the 2, 4 and 6 GB respectively. This correlates also well with the results of molecular dynamics simulations for vacancies and the step edge as shown in Fig. S4 in the ESI. From a quantitative point of view, the dissociation rate increased by 50% to 70% in the presence of grain boundaries compared to the non-defective surface. This result gives indication that metal dusting corrosion is much higher in a system where the surface exposes a polycrystalline cleave at ambient temperature, which is the case in many industrial applications.

At 800 K, a high dissociation rate was recorded irrespective of the roughness of the surface. A visualisation of the MD simulation trajectory confirms that CO molecules dissociate at a rapid rate followed by the diffusion of carbon atoms from surface to sub-surface leaving their adsorption site vacant to the next CO molecule. Interestingly, the difference between clean and defective surfaces is negligible near or far from the surface defects at this simulated temperature probably because the probabilities of CO dissociation are similar at elevated temperatures.

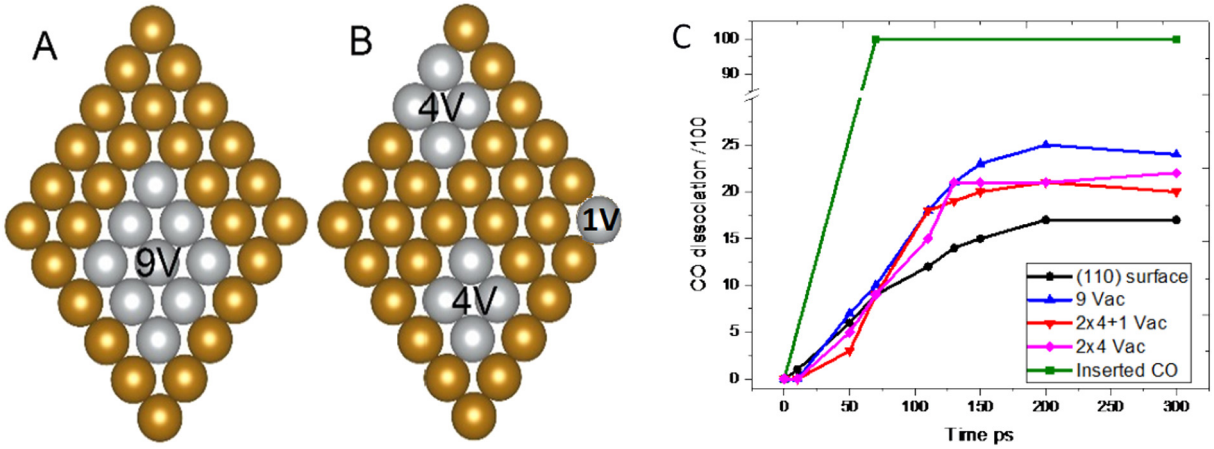

Fig. 4. (A) A 9-vacancy cluster (B) two- 4 vacancy clusters on a (110) surface plus single vacancy. (C) CO dissociation rates for CO on defected surfaces in comparison with a clean surface at 500 K.

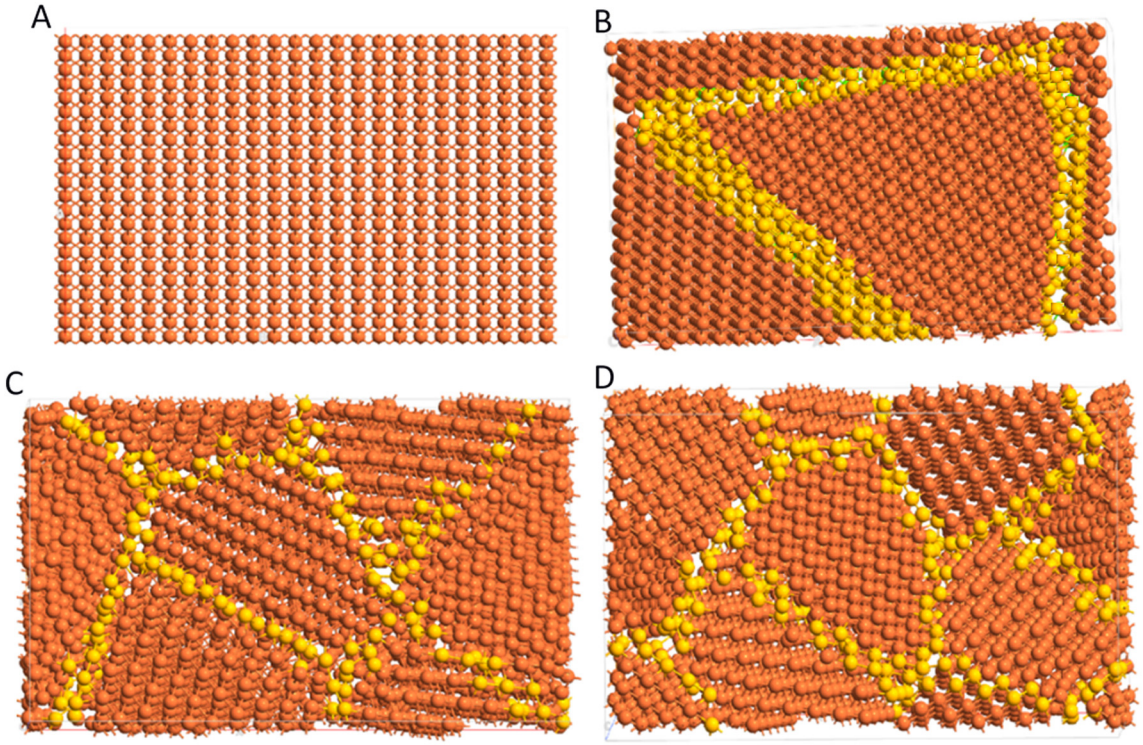

Fig. 5. Top view of different surface topologies (before relaxation), used to examine the CO dissociation rate. (A) clean (110) surface, (B) a two-grain system, (C) a four-grain system, (D) a six grain system. Different colours are used to emphasize the grain boundaries.

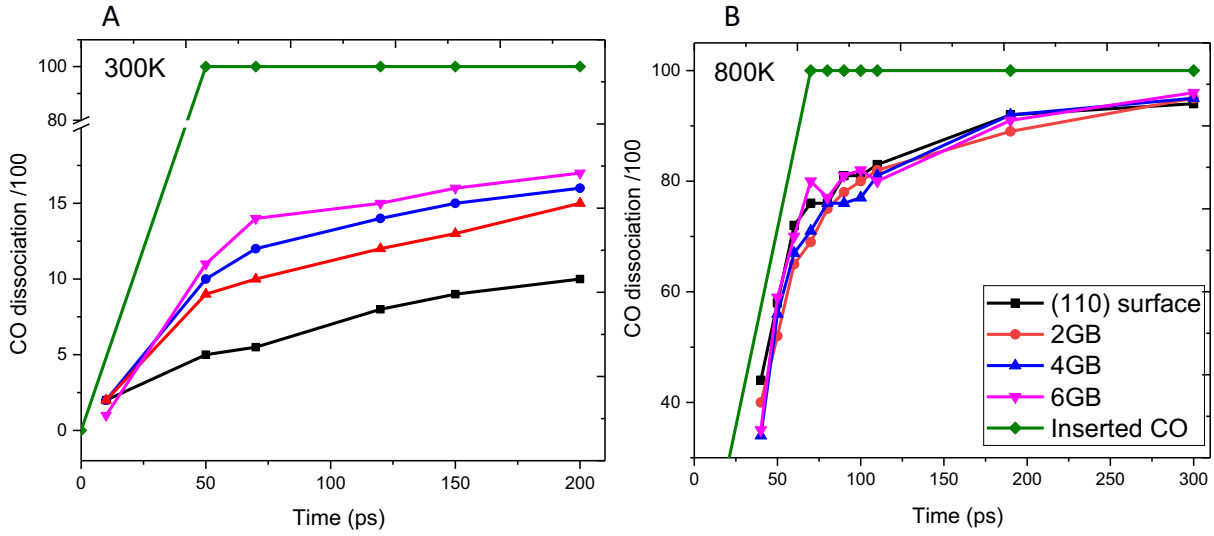

Fig. 6. CO dissociation rate as function of simulation time at 300 K (left) and 800 K (right). The data corresponding to a clean (110) surface are in black, those for a two-grain system in red, for 4 grain system in blue and those for the system with 6 grains in pink. The green line represents the number of inserted molecules. (For interpretation of the references to color in this figure legend, the reader is referred to the web version of this article.)

4. Conclusions

The adsorption and dissociation of CO on Fe surface in the presence of various surface extended defects have been fully characterized using the ReaxFF potential and duly tested against DFT results. We demonstrated that CO molecules adsorbed near defective Fe surfaces containing vacancy clusters develop stronger Fe—C bond and weaker C—O bond resulting in lower dissociation barriers and shorter pathways. By means of molecular dynamics, we demonstrated that the adsorption of molecular CO is increased considerably by the presence of extended defects on the surface that create lower energy adsorption sites at the defect edges and increase the number of adsorbed molecules at a given surface area. We also showed that large vacancy cluster defects enhance CO adsorption and dissociation in a manner similar to single vacancy defects but with higher dissociation rates for a given surface area. The CO dissociation rates calculated for grain boundaries emerging on the surfaces show that the increase in number of grain boundaries exposed to the surface leads to an increase in dissociation rates by up to 70% at ambient temperature. This computational study shows that extended surface defects boost metal dusting corrosion significantly, indicating thus that it is necessary to build large scale simulations to study the inhibition process of metal dusting in the presence of the inevitable

extended surface defects.

Acknowledgement

This work is supported by the Qatar National Research Fund (QNRF) through the National Priorities Research Program (NPRP 10-0105-170118). The advanced computing facility of Texas A&M University at Qatar is used for all calculations.

Appendix A. Supplementary data

Supplementary data to this article can be found online at https://doi.org/10.1016/j.apsusc.2019.05.278.

References

[1] C.S. Becquart, J.M. Raulot, G. Bencteux, C. Domain, M. Perez, S. Garruchet, H. Nguyen, Atomistic modeling of an Fe system with a small concentration of C, Comput. Mater. Sci. 40 (2007) 119–129, https://doi.org/10.1016/j.commatsci.2006.11.005.
[2] J. Zhang, D.J. Young, Kinetics and mechanisms of nickel metal dusting I. Kinetics and morphology, Corros. Sci. 49 (2007) 1496–1512.
[3] C. Chun, J. Mumford, T. Ramanarayanan, On the mechanism of metal dusting corrosion, High Temp. Mater. Proc. a Symp. Honor 65th Birthd. Profr. Wayne L. Worrell, The Electrochemical Society, 2002, p. 247.
[4] M.R. Elahifard, M.P. Jigato, J.W. Niemantsverdriet, Direct versus hydrogen-assisted CO dissociation on the Fe (100) surface: a DFT study, ChemPhysChem 13 (2012) 89–91.
[5] S. Liu, Y.W. Li, J. Wang, H. Jiao, Reactions of CO, H2O, CO2, and H2 on the clean and precovered Fe(110) surfaces - a DFT investigation, J. Phys. Chem. C 119 (2015) 28377–28388, https://doi.org/10.1021/acs.jpcc.5b07497.
[6] A. Chakrabarty, O. Bouhali, N. Mousseau, C.S. Becquart, F. El-Mellouhi, Influence of surface vacancy defects on the carburisation of Fe 110 surface by carbon monoxide, J. Chem. Phys. 145 (2016) 44710, , https://doi.org/10.1063/1.4958966.
[7] E.T. Bentria, G.K. N'tsouaglo, C.S. Becquart, O. Bouhali, N. Mousseau, F. El-Mellouhi, The role of emerging grain boundary at iron surface, temperature and hydrogen on metal dusting initiation, Acta Mater. 135 (2017), https://doi.org/10.1016/j.actamat.2017.06.049.
[8] C.S. Becquart, C. Domain, Modeling microstructure and irradiation effects, Met. Mater. Trans. A 42 (2011) 852–870, https://doi.org/10.1007/s11661-010-0460-7.
[9] Y. Fukai, K. Mori, H. Shinomiya, The phase diagram and superabundant vacancy formation in Fe–H alloys under high hydrogen pressures, J. Alloys Compd. 348 (2003) 105.
[10] A. Vehanen, P. Hautojärvi, J. Johansson, J. Yli-Kauppila, P. Moser, Vacancies and carbon impurities in α-iron: electron irradiation, Phys. Rev. B 25 (1982) 762.
[11] D. Tanguy, M. Mareschal, Superabundant vacancies in a metal-hydrogen system: Monte Carlo simulations, Phys. Rev. B 72 (2005) 174116.
[12] C.S. Becquart, V. Pontikis, Grain boundary intersecting a free surface. Structural evolution toward equilibrium, Mater. Sci. Forum 294–296 (1999) 625–628, https://doi.org/10.4028/www.scientific.net/MSF.294-296.625.
[13] C. Domain, Ab initio modeling of defect properties with substitutional and interstitials elements in steels and Zr alloys, J. Nucl. Mater. 351 (2006) 1–19, https://doi.org/10.1016/j.jnucmat.2006.02.025.
[14] V. Maurice, P. Marcus, Progress in corrosion science at atomic and nanometric scales, Prog. Mater. Sci. 95 (2018) 132–171.
[15] K. Lu, C.-F. Huo, Y. He, J. Yin, J. Liu, Q. Peng, W.-P. Guo, Y. Yang, Y.-W. Li, X.-D. Wen, Grain boundary plays a key role in carbon diffusion in carbon irons revealed by a ReaxFF study, J. Phys. Chem. C 122 (2018) 23191–23199.
[16] T.P. Senftle, S. Hong, M.M. Islam, S.B. Kylasa, Y. Zheng, Y.K. Shin, C. Junkermeier, R. Engel-Herbert, M.J. Janik, H.M. Aktulga, The ReaxFF reactive force-field: development, applications and future directions, Npj Comput. Mater. 2 (2016) 15011.
[17] P. Hohenberg, W. Kohn, Inhomogeneous electron gas, Phys. Rev. 136 (1964) B864.
[18] G. Kresse, J. Hafner, Norm-conserving and ultrasoft pseudopotentials for first-row and transition elements, J. Phys. Condens. Matter 6 (1994) 8245.
[19] P.E. Blöchl, Projector augmented-wave method, Phys. Rev. B 50 (1994) 17953.
[20] J.P. Pedrew, K. Burke, M. Ernzerhof, Phys. Rev. Lett. 77 (1996) 3865.
[21] Www.quantumwise.com, (2015) Virtual NanoLab.
[22] Z. Fan, Y. Wu, X. Zhao, Y. Lu, Simulation of polycrystalline structure with Voronoi diagram in Laguerre geometry based on random closed packing of spheres, Comput. Mater. Sci. 29 (2004) 301–308.
[23] G. Henkelman, H. Jónsson, A climbing image nudged elastic band method for finding saddle points and minimum energy paths, J. Chem. Phys. 113 (2000) 9901.
[24] S. Smidstrup, A. Pedersen, K. Stokbro, H. Jónsson, Improved initial guess for minimum energy path calculations, J. Chem. Phys. 140 (2014) 214106.
[25] P. Błoński, A. Kiejna, Structural, electronic, and magnetic properties of bcc iron surfaces, Surf. Sci. 601 (2007) 123–133.
[26] G. Liu, D. Nguyen-Manh, B.G. Liu, D.G. Pettifor, Magnetic properties of point defects in iron within the tight-binding-bond Stoner model, Phys. Rev. B 71 (17) (2005) 174115.
[27] C.S. Becquart, C. Domain, J. Foct, Ab initio calculations of some atomic and point defect interactions involving C and N in Fe, Philos. Mag. 85 (2005) 533–540, https://doi.org/10.1080/02678370412331320152.
[28] P.A. Korzhavyi, I.A. Abrikosov, B. Johansson, First-principles calculations of the vacancy formation energy in transition and noble metals, Phys. Rev. B 59 (1999) 11693.
[30] A.D. Rollett, D. Saylor, J. Fridy, B.S. El-Dasher, A. Brahme, S. Lee, C. Cornwell, R. Noack, Modeling polycrystalline microstructures in 3D, AIP Conf. Proc., AIP, 2004, pp. 71–77.